Multiterminal multimode spin-dependent scattering matrix formalism: Electron and hole quantum spin transport in multiterminal junctions

P. Brusheim,[1,*] D. Csontos,[2] U. Zülicke,[2] and H. Q. Xu[1,†]
[1]*Division of Solid State Physics, Lund University, Box 118, S-22100 Lund, Sweden*
[2]*Institute of Fundamental Sciences and MacDiarmid Institute for Advanced Materials and Nanotechnology, Massey University, Private Bag 11 222, Palmerston North 4442, New Zealand*

(Received 22 May 2008; revised manuscript received 25 June 2008; published 1 August 2008)

We present a derivation of a scattering matrix method providing an exact multimode solution to spin-dependent quantum transport in multiterminal structures. The method is formulated in a general language such that it can readily be applied to any spin-*S* system with spin interactions. We apply the formalism to spin-1/2 electron and spin-3/2 hole transport in three- and four-terminal structures. It is shown that the existence of a third lead lifts constraints on the flux polarization of two-terminal electron transport. A spin-rectification property in a three-terminal system with Rashba spin-orbit interaction is demonstrated. We furthermore find that a four-terminal structure can partition a fully spin-polarized electron flux into two oppositely polarized fluxes. For holes, we calculate the polarization vector of both the injected states as well as the outgoing states in a three-terminal structure. Close to the onset of propagating channels, the hole polarization exhibits peak-dip structures attributed to the angular-momentum dependent Fano resonances in the three-terminal junction. We rigorously show that when the outgoing state is restricted to a single channel, the polarization is uniquely determined by the outgoing lead state, independent of the scattering details of the structure.

DOI: 10.1103/PhysRevB.78.085301 PACS number(s): 72.10.−d, 71.70.Ej, 73.23.−b, 72.25.−b

I. INTRODUCTION

Theoretical understanding of phase-coherent quantum transport in multiterminal structures was advanced by Büttiker,[1] who realized that all terminals in such a quantum system should be treated on an equal footing. Inspired by this, theoretical investigations,[2–19] as well as experimental investigations[20–27] have since been undertaken to study charge transport in low-dimensional multiterminal structures.

Today, the subject of spin-dependent transport in multiterminal structures with spin-orbit interaction (SOI) has become an area of research, which attracts great attention due to the occurrence of interesting SOI-induced spin polarization[28–31] and noise phenomena[32] in the structures. To treat spin-dependent quantum transport in multiterminal nanostructures accurately, interchannel interactions, which were completely neglected in Refs. 28–31 while only treated perturbatively in Ref. 32, needs to be fully included. This calls for a stable numerical method since no closed-form solution exists for confined SOI systems. Green's function approaches, which are formulated based on real-space lattice models, have been employed to study spin-dependent quantum transport in multiterminal systems.[33–36] These studies have, however, largely been limited to devices with simple geometrical structures. This is possibly due to numerical difficulties in treating multiterminal systems with complicated geometrical structures and the resulting tight-binding Hamiltonians in Green's function approaches.

In this paper we will derive an exact multiterminal multichannel scattering matrix method for spin-dependent quantum transport. The method is formulated in a general language, which allows for applications to electron transport, as well as to hole transport, in confined mesoscopic systems with complex geometries and can easily be extended to finite temperatures.[37] We will utilize the presented method to study spin angular-momentum polarization of transported carriers in three- and four-terminal structures. It is found that the presence of a third lead lifts some of the symmetry constraints on the spin-polarization properties derived within the two-terminal theory. Our numerical calculations are verified by an analytical derivation of the symmetry constraints on the spin-dependent transport in multiterminal structures. In particular, we demonstrate an electron-spin rectification in a three-terminal structure as well as a partitioning of a fully spin-polarized flux into two oppositely polarized fluxes in a four-terminal structure. For holes it is found that the outgoing states in a three-terminal structure is largely unpolarized, except to those close to the opening of the transmission channels, where the angular-momentum Fano interactions give rise to the peak-dip features in the polarization. Furthermore, it is shown that when the outgoing lead only supports a single channel, the carrier polarization is independent of the scattering details of the system.

The paper is organized as follows: In Sec. II, we will present the spin-resolved scattering matrix formalism for multichannel multiterminal transport. By formulating it in a general spinor language it does not depend on the explicit form of the Hamiltonian and is therefore able to treat both electron and hole transports on an equal footing. In Sec. III, we will apply the formalism to the study of spin-resolved electron transport in three- and four-terminal structures with Rashba spin-orbit interaction, and in Sec. IV, the formalism is applied to the hole transport in a three-terminal junction. Conclusions are presented in Sec. V.

II. FORMALISM

A. Scattering matrices in the individual branches

We set out to derive a scattering matrix formalism for a multiterminal structure by briefly introducing the procedure

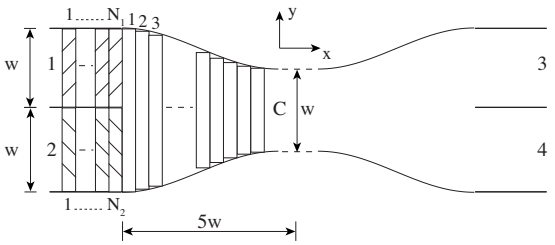

FIG. 1. Schematic of a three- and four-terminal system. The left side represents the three-terminal junction, which can be connected to another junction (right side) to form a four-terminal structure. The system is divided into slices in the transport direction and a local basis is used in each slice. The scale arrows indicate measures used for the numerical calculations in Secs. III and IV.

of deriving two-terminal scattering matrices in the individual branches. Our model multiterminal structure is shown in Fig. 1, which consists of five branches labeled as 1–4 and *C*. The multiterminal system is divided into a large number of slices along the transport direction *x* depicted in Fig. 1, such that in each slice, any device-characteristic parameter can be treated as a constant along the transport direction. By representing the Hamiltonian in a local complete spinor basis $\{|\chi_{\sigma n}^{\lambda(i)}\rangle\}$, where n labels the spatial degrees of freedom and σ labels the spinor components, the eigensolutions in slice i of branch λ at a given Fermi energy can be found and written as

$$\phi_\alpha^{\lambda(i)} = e^{ik_\alpha^{\lambda(i)}x} \sum_{\sigma n} d_{\alpha,\sigma n}^{\lambda(i)} |\chi_{\sigma n}^{\lambda(i)}\rangle. \tag{1}$$

The scattering wave function in slice i of branch λ can, hence, be written as

$$\Psi^{\lambda(i)} = \sum_{\alpha,\sigma n} [a_\alpha^{\lambda(i),I} d_{\alpha,\sigma n}^{\lambda(i),I} e^{ik_\alpha^{\lambda(i),I}x} + a_\alpha^{\lambda(i),II} d_{\alpha,\sigma n}^{\lambda(i),II} e^{ik_\alpha^{\lambda(i),II}x}] |\chi_{\sigma n}^{\lambda(i)}\rangle. \tag{2}$$

Here we have separated the eigensolutions $\{\phi_\alpha^{\lambda(i)}\}$ into a set $\{\phi_\alpha^{\lambda(i),I}\}$ with $I=\{\alpha|\Im[k_\alpha^{\lambda(i)}]=0\wedge v_\alpha^{\lambda(i)}>0\vee\Im[k_\alpha^{\lambda(i)}]>0\}$, consisting of forward propagating or evanescent modes and a set $\{\phi_\alpha^{\lambda(i),II}\}$ with $II=\{\alpha|\Im[k_\alpha^{\lambda(i)}]=0\wedge v_\alpha^{\lambda(i)}<0\vee\Im[k_\alpha^{\lambda(i)}]<0\}$, consisting of backward propagating or exploding modes, where $v_\alpha^{\lambda(i)}$ is the velocity expectation value of mode $\phi_\alpha^{\lambda(i)}$. By imposing continuity requirements on the wave function and the flux between every two adjacent slices, a scattering matrix for a two-terminal structure was derived in Ref. 38. This formalism can readily be applied on each individual branch λ, generating a scattering matrix $\boldsymbol{S}^\lambda(i,j)$, which connects the amplitudes of the wave function in any two slices i and j in the branch,

$$\begin{bmatrix} \boldsymbol{A}_I^{\lambda(i)} \\ \boldsymbol{A}_{II}^{\lambda(j)} \end{bmatrix} = \boldsymbol{S}^\lambda(i,j) \begin{bmatrix} \boldsymbol{A}_I^{\lambda(j)} \\ \boldsymbol{A}_{II}^{\lambda(i)} \end{bmatrix}, \tag{3}$$

where $\boldsymbol{A}_I^{\lambda(i)}$ and $\boldsymbol{A}_{II}^{\lambda(i)}$ are coefficient vectors containing $\{a_\alpha^{\lambda(i),I}\}$ and $\{a_\alpha^{\lambda(i),II}\}$, respectively. By setting $\boldsymbol{S}^\lambda=\boldsymbol{S}^\lambda(1,N_\lambda)$, we can write the full two-terminal scattering matrix equations, which relate the amplitudes of the waves at slices 1 and N_1 of branch 1 and the amplitudes of the waves at slices 1 and N_2 of branch 2, respectively, as

$$\begin{bmatrix} \boldsymbol{A}_I^{1(N_1)} \\ \boldsymbol{A}_{II}^{1(1)} \end{bmatrix} = \begin{pmatrix} \boldsymbol{S}_{11}^1 & \boldsymbol{S}_{12}^1 \\ \boldsymbol{S}_{21}^1 & \boldsymbol{S}_{22}^1 \end{pmatrix} \begin{bmatrix} \boldsymbol{A}_I^{1(1)} \\ \boldsymbol{A}_{II}^{1(N_1)} \end{bmatrix}, \tag{4}$$

$$\begin{bmatrix} \boldsymbol{A}_I^{2(N_2)} \\ \boldsymbol{A}_{II}^{2(1)} \end{bmatrix} = \begin{pmatrix} \boldsymbol{S}_{11}^2 & \boldsymbol{S}_{12}^2 \\ \boldsymbol{S}_{21}^2 & \boldsymbol{S}_{22}^2 \end{pmatrix} \begin{bmatrix} \boldsymbol{A}_I^{2(1)} \\ \boldsymbol{A}_{II}^{2(N_2)} \end{bmatrix}. \tag{5}$$

The two-terminal scattering matrix equations for the central branch and the two right branches, i.e., branches 3 and 4, can be derived in the same way. For further details of the derivation of the scattering matrix for a two-terminal electron system in the presence of a SOI, we refer to Ref. 38; while for a two-terminal hole system, we refer to Sec. IV.

B. Three-terminal scattering matrix

We will now present our derivation of the scattering matrix for a three-terminal quantum structure. Consider a device shown in the left half of Fig. 1. At the three-terminal intersection where branches 1 and 2 connect with branch *C*, the relations between the expansion coefficients of the wave function in slice N_1 of branch 1, slice N_2 of branch 2, and slice 1 of branch *C* can be obtained by imposing continuity requirements on the wave function and the flux. This can be written in the form of a matrix equation as

$$\begin{pmatrix} \boldsymbol{P}_I & \boldsymbol{P}_{II} \\ \boldsymbol{Q}_I & \boldsymbol{Q}_{II} \end{pmatrix} \begin{pmatrix} \boldsymbol{\Gamma}_I & \boldsymbol{0} \\ \boldsymbol{0} & \boldsymbol{\Gamma}_{II} \end{pmatrix} \begin{Bmatrix} [\boldsymbol{A}_I^{L(N)}] \\ [\boldsymbol{A}_{II}^{L(N)}] \end{Bmatrix} = \begin{bmatrix} \boldsymbol{D}_I^{C(1)} & \boldsymbol{D}_{II}^{C(1)} \\ \boldsymbol{R}_I & \boldsymbol{R}_{II} \end{bmatrix} \begin{bmatrix} \boldsymbol{A}_I^{C(1)} \\ \boldsymbol{A}_{II}^{C(1)} \end{bmatrix}. \tag{6}$$

Here, to simplify the notation, we define $[\boldsymbol{A}_I^{L(N)}]=[\boldsymbol{A}_I^{1(N_1)},\boldsymbol{A}_I^{2(N_2)}]^T$ and $[\boldsymbol{A}_{II}^{L(N)}]=[\boldsymbol{A}_{II}^{1(N_1)},\boldsymbol{A}_{II}^{2(N_2)}]^T$. The explicit forms of the matrices in Eq. (6) are given by

$$[\boldsymbol{D}_{I\{II\}}^{\lambda(i)}]_{\sigma n,\alpha} = d_{\alpha,\sigma n}^{\lambda(i),I\{II\}},$$

$$\boldsymbol{P}_{I\{II\}} = [\boldsymbol{F}^1 D_{I(II)}^{1(N_1)}, \boldsymbol{F}^2 D_{I(II)}^{2(N_2)}],$$

$$\boldsymbol{Q}_{I\{II\}} = \begin{bmatrix} \boldsymbol{Q}_{I(II)}^{1(N_1)} & \boldsymbol{0} \\ \boldsymbol{0} & \boldsymbol{Q}_{I(II)}^{2(N_2)} \end{bmatrix},$$

$$\boldsymbol{R}_{I\{II\}} = \begin{bmatrix} (\boldsymbol{F}^1)^T \boldsymbol{Q}_{I(II)}^{C(1)} \\ (\boldsymbol{F}^2)^T \boldsymbol{Q}_{I(II)}^{C(1)} \end{bmatrix},$$

$$\boldsymbol{\Gamma}_{I\{II\}} = \begin{bmatrix} \gamma_{I(II)}^{1(N_1)} & \boldsymbol{0} \\ \boldsymbol{0} & \gamma_{I(II)}^{2(N_2)} \end{bmatrix}, \tag{7}$$

where

$$(\boldsymbol{F}^\lambda)_{\sigma' n',\sigma n} = \langle \chi_{\sigma' n'}^{C(1)} | \chi_{\sigma n}^{\lambda(N_\lambda)} \rangle, \tag{8}$$

is the matrix of the overlap integrals between the basis functions in slice N_λ of branch λ and the basis functions in slice 1 of branch *C*, $\boldsymbol{\gamma}_I^{\lambda(N_\lambda)}$ and $\boldsymbol{\gamma}_{II}^{\lambda(N_\lambda)}$ are the diagonal matrices consisting of elements $\{\exp[ik_\alpha^{\lambda(N_\lambda),I} l^{(N_\lambda)}]\delta_{\alpha'\alpha}\}$ and $\{\exp[ik_\alpha^{\lambda(N_\lambda),II} l^{(N_\lambda)}]\delta_{\alpha'\alpha}\}$, respectively, with $l^{(N_\lambda)}$ denoting the longitudinal length of stripe N_λ in branch λ, and $\boldsymbol{Q}_I^{\lambda(i)}$ and

$\boldsymbol{Q}_{II}^{\lambda(i)}$ are the flux matrices, which can be formally written as $\boldsymbol{Q}_{I}^{\lambda(i)}=\boldsymbol{v}_{I}^{\lambda(i)}\boldsymbol{D}_{I}^{\lambda(i)}$ and $\boldsymbol{Q}_{II}^{\lambda(i)}=\boldsymbol{v}_{II}^{\lambda(i)}\boldsymbol{D}_{II}^{\lambda(i)}$. Here, $\boldsymbol{v}_{I}^{\lambda(i)}$ and $\boldsymbol{v}_{II}^{\lambda(i)}$ are the velocity matrices. The forms of the velocity matrices depend on the Hamiltonian (see, for example, Refs. 38–40) and will thus be specified in later sections, where explicit systems are considered.

In deriving Eq. (6), we have assumed that the transverse width of the central branch at the interface contains the transverse extensions of both branches 1 and 2 (see Fig. 1). It is important here to note that the matrix equation that describes the matching of the wave function needs to be projected onto the basis functions whose transverse extensions contain both sides of the matched domain; whereas the matrix equations that describe the matching of the flux need to be projected onto the basis functions having the smaller transverse extensions.[12] After some algebra[41] we find

$$\boldsymbol{A}_{I}^{C(1)}=\boldsymbol{U}[\boldsymbol{A}_{I}^{L(N)}]+\boldsymbol{V}\boldsymbol{A}_{II}^{C(1)},$$

$$[\boldsymbol{A}_{II}^{L(N)}]=\boldsymbol{\Gamma}_{II}^{-1}\boldsymbol{Q}_{II}^{-1}\times\{(\boldsymbol{R}_{I}\boldsymbol{U}-\boldsymbol{Q}_{I}\boldsymbol{\Gamma}_{I})[\boldsymbol{A}_{I}^{L(N)}]+(\boldsymbol{R}_{I}\boldsymbol{V}+\boldsymbol{R}_{II})\boldsymbol{A}_{II}^{C(1)}\},\tag{9}$$

with

$$\boldsymbol{U}=[\boldsymbol{D}_{I}^{C(1)}-\boldsymbol{P}_{II}\boldsymbol{Q}_{II}^{-1}\boldsymbol{R}_{I}]^{-1}(\boldsymbol{P}_{I}-\boldsymbol{P}_{II}\boldsymbol{Q}_{II}^{-1}\boldsymbol{Q}_{I})\boldsymbol{\Gamma}_{I},$$

$$\boldsymbol{V}=[\boldsymbol{D}_{I}^{C(1)}-\boldsymbol{P}_{II}\boldsymbol{Q}_{II}^{-1}\boldsymbol{R}_{I}]^{-1}[\boldsymbol{P}_{II}\boldsymbol{Q}_{II}^{-1}\boldsymbol{R}_{II}-\boldsymbol{D}_{II}^{C(1)}].\tag{10}$$

Equation (9) relates the amplitudes of the outgoing, propagating, and decaying waves to the amplitudes of incoming, propagating, and exploding waves at the connection interface of the three branches. To relate the amplitudes of the waves in the leads connecting to branches 1 and 2 to the amplitudes of the waves in the central branch, we cast Eqs. (4) and (5) into

$$\begin{Bmatrix}[\boldsymbol{A}_{I}^{L(N)}]\\ [\boldsymbol{A}_{II}^{L(1)}]\end{Bmatrix}=\begin{pmatrix}\boldsymbol{S}_{11}^{1} & \boldsymbol{0} & \boldsymbol{S}_{12}^{1} & \boldsymbol{0}\\ \boldsymbol{0} & \boldsymbol{S}_{11}^{2} & \boldsymbol{0} & \boldsymbol{S}_{12}^{2}\\ \boldsymbol{S}_{21}^{1} & \boldsymbol{0} & \boldsymbol{S}_{22}^{1} & \boldsymbol{0}\\ \boldsymbol{0} & \boldsymbol{S}_{21}^{2} & \boldsymbol{0} & \boldsymbol{S}_{22}^{2}\end{pmatrix}\begin{Bmatrix}[\boldsymbol{A}_{I}^{L(1)}]\\ [\boldsymbol{A}_{II}^{L(N)}]\end{Bmatrix}=\begin{pmatrix}\boldsymbol{S}_{11} & \boldsymbol{S}_{12}\\ \boldsymbol{S}_{21} & \boldsymbol{S}_{22}\end{pmatrix}\begin{Bmatrix}[\boldsymbol{A}_{I}^{L(1)}]\\ [\boldsymbol{A}_{II}^{L(N)}]\end{Bmatrix}.\tag{11}$$

Inserting this equation into Eq. (9), we find

$$\boldsymbol{A}_{I}^{C(1)}=\boldsymbol{U}[\boldsymbol{S}_{11}+\boldsymbol{S}_{12}\boldsymbol{X}(\boldsymbol{R}_{I}\boldsymbol{U}-\boldsymbol{Q}_{I}\boldsymbol{\Gamma}_{I})\boldsymbol{S}_{11}][\boldsymbol{A}_{I}^{L(1)}]+[\boldsymbol{U}\boldsymbol{S}_{12}\boldsymbol{X}(\boldsymbol{R}_{I}\boldsymbol{V}+\boldsymbol{R}_{II})+\boldsymbol{V}]\boldsymbol{A}_{II}^{C(1)},$$

$$[\boldsymbol{A}_{II}^{L(1)}]=[\boldsymbol{S}_{22}\boldsymbol{X}(\boldsymbol{R}_{I}\boldsymbol{U}-\boldsymbol{Q}_{I}\boldsymbol{\Gamma}_{I})\boldsymbol{S}_{11}+\boldsymbol{S}_{21}][\boldsymbol{A}_{I}^{L(1)}]+\boldsymbol{S}_{22}\boldsymbol{X}(\boldsymbol{R}_{I}\boldsymbol{V}+\boldsymbol{R}_{II})\boldsymbol{A}_{II}^{C(1)},\tag{12}$$

where

$$\boldsymbol{X}=[\mathbb{1}-\boldsymbol{\Gamma}_{II}^{-1}\boldsymbol{Q}_{II}^{-1}(\boldsymbol{R}_{I}\boldsymbol{U}-\boldsymbol{Q}_{I}\boldsymbol{\Gamma}_{I})\boldsymbol{S}_{12}]^{-1}\boldsymbol{\Gamma}_{II}^{-1}\boldsymbol{Q}_{II}^{-1}.\tag{13}$$

This leads to a three-terminal scattering matrix $\boldsymbol{\Sigma}^{3T}$, which relates the amplitudes of the outgoing and decaying waves in the first slices of branches 1, 2, and C to the amplitudes of the incoming and exploding waves in these branch slices,

$$\begin{Bmatrix}\boldsymbol{A}_{I}^{C(1)}\\ [\boldsymbol{A}_{II}^{L(1)}]\end{Bmatrix}=\begin{pmatrix}\boldsymbol{\Sigma}_{11}^{3T} & \boldsymbol{\Sigma}_{12}^{3T}\\ \boldsymbol{\Sigma}_{21}^{3T} & \boldsymbol{\Sigma}_{22}^{3T}\end{pmatrix}\begin{bmatrix}[\boldsymbol{A}_{I}^{L(1)}]\\ \boldsymbol{A}_{II}^{C(1)}\end{bmatrix},\tag{14}$$

with

$$\boldsymbol{\Sigma}_{11}^{3T}=\boldsymbol{U}[\boldsymbol{S}_{11}+\boldsymbol{S}_{12}\boldsymbol{X}(\boldsymbol{R}_{I}\boldsymbol{U}-\boldsymbol{Q}_{I}\boldsymbol{\Gamma}_{I})\boldsymbol{S}_{11}],$$

$$\boldsymbol{\Sigma}_{12}^{3T}=\boldsymbol{U}\boldsymbol{S}_{12}\boldsymbol{X}(\boldsymbol{R}_{I}\boldsymbol{V}+\boldsymbol{R}_{II})+\boldsymbol{V},$$

$$\boldsymbol{\Sigma}_{21}^{3T}=\boldsymbol{S}_{22}\boldsymbol{X}(\boldsymbol{R}_{I}\boldsymbol{U}-\boldsymbol{Q}_{I}\boldsymbol{\Gamma}_{I})\boldsymbol{S}_{11}+\boldsymbol{S}_{21},$$

$$\boldsymbol{\Sigma}_{22}^{3T}=\boldsymbol{S}_{22}\boldsymbol{X}(\boldsymbol{R}_{I}\boldsymbol{V}+\boldsymbol{R}_{II}).\tag{15}$$

This scattering matrix can now be iterated over the slices in branch C by the standard scheme described in Ref. 39 to generate the complete scattering matrix $\boldsymbol{S}^{3T}$ for the three-terminal system,

$$\begin{Bmatrix}\boldsymbol{A}_{I}^{C(N_C)}\\ [\boldsymbol{A}_{II}^{L(1)}]\end{Bmatrix}=\begin{pmatrix}\boldsymbol{S}_{11}^{3T} & \boldsymbol{S}_{12}^{3T}\\ \boldsymbol{S}_{21}^{3T} & \boldsymbol{S}_{22}^{3T}\end{pmatrix}\begin{Bmatrix}[\boldsymbol{A}_{I}^{L(1)}]\\ \boldsymbol{A}_{II}^{C(N_C)}\end{Bmatrix}.\tag{16}$$

In this equation, we have expressed the amplitudes of the outgoing and decaying waves in the first slices of branches 1 and 2 and the N_Cth slice of branch C in terms of the amplitudes of the incoming and exploding waves in these slices. A similar three-terminal scattering matrix equation can be derived for the three-branch structure shown in the right half of Fig. 1, consisting of the central branch and the branches 3 and 4.

C. Four-terminal scattering matrix

In order to generate a four-terminal scattering matrix for the multiterminal structure shown in Fig. 1, we make use of our progress so far [Eq. (16)] and consider the wave function and flux continuity requirements at the second three-branch junction. At this junction interface, the presented procedure for deriving the three-terminal scattering matrix can once more be used. However, it must be employed in the reversed order, going from the central branch to the branches 3 and 4. We write this as

$$\begin{bmatrix}\boldsymbol{D}_{I}^{C(N_C)} & \boldsymbol{D}_{II}^{C(N_C)}\\ \tilde{\boldsymbol{R}}_{I} & \tilde{\boldsymbol{R}}_{II}\end{bmatrix}\begin{pmatrix}\tilde{\boldsymbol{\Gamma}}_{I} & \boldsymbol{0}\\ \boldsymbol{0} & \tilde{\boldsymbol{\Gamma}}_{II}\end{pmatrix}\begin{bmatrix}\boldsymbol{A}_{I}^{C(N_C)}\\ \boldsymbol{A}_{II}^{C(N_C)}\end{bmatrix}=\begin{pmatrix}\tilde{\boldsymbol{P}}_{I} & \tilde{\boldsymbol{P}}_{II}\\ \tilde{\boldsymbol{Q}}_{I} & \tilde{\boldsymbol{Q}}_{II}\end{pmatrix}\begin{Bmatrix}[\boldsymbol{A}_{I}^{R(1)}]\\ [\boldsymbol{A}_{II}^{R(1)}]\end{Bmatrix},\tag{17}$$

where $[\boldsymbol{A}_{I\{II\}}^{R(1)}]=[\boldsymbol{A}_{I\{II\}}^{3(1)},\boldsymbol{A}_{I\{II\}}^{4(1)}]^{T}$ are the coefficient vectors in the leftmost slices, connecting to the central branch in branches 3 and 4, and

$$\tilde{\boldsymbol{P}}_{I\{II\}}=[\tilde{\boldsymbol{F}}^{3}\boldsymbol{D}_{I(II)}^{3(1)},\tilde{\boldsymbol{F}}^{4}\boldsymbol{D}_{I(II)}^{4(1)}],$$

$$\tilde{\boldsymbol{Q}}_{I\{II\}}=\begin{bmatrix}\boldsymbol{Q}_{I(II)}^{3(1)} & \boldsymbol{0}\\ \boldsymbol{0} & \boldsymbol{Q}_{I(II)}^{4(1)}\end{bmatrix},$$

$$\tilde{R}_{I\{II\}}=\begin{bmatrix}(\tilde{\boldsymbol{F}}^{3})^{T}\boldsymbol{Q}_{I(II)}^{C(N_C)}\\ (\tilde{\boldsymbol{F}}^{4})^{T}\boldsymbol{Q}_{I(II)}^{C(N_C)}\end{bmatrix},$$

$$\tilde{\boldsymbol{\Gamma}}_{I\{II\}} = \begin{bmatrix} \boldsymbol{\gamma}_{I(II)}^{C(N_C)} & \mathbf{0} \\ \mathbf{0} & \boldsymbol{\gamma}_{I(II)}^{C(N_C)} \end{bmatrix}, \tag{18}$$

where the overlap integral matrix is now given by

$$(\tilde{\boldsymbol{F}}^{\lambda})_{\sigma' n', \sigma n} = \langle \chi_{\sigma' n'}^{C(N_C)} | \chi_{\sigma n}^{\lambda(1)} \rangle, \tag{19}$$

and matrices $\boldsymbol{D}_I^{\lambda(i)}$ and $\boldsymbol{D}_{II}^{\lambda(i)}$, $\boldsymbol{\gamma}_I^C$ and $\boldsymbol{\gamma}_{II}^C$, and $\boldsymbol{Q}_I^{\lambda(i)}$ and $\boldsymbol{Q}_{II}^{\lambda(i)}$, with $\lambda = 3$, 4, or C, are defined as in Eq. (7). After some algebra, Eq. (17) can be written as

$$[\boldsymbol{A}_I^{R(1)}] = \tilde{\boldsymbol{U}} \boldsymbol{A}_I^{C(N_C)} + \tilde{\boldsymbol{V}} [\boldsymbol{A}_{II}^{R(1)}],$$

$$\boldsymbol{A}_{II}^{C(N_C)} = \tilde{\boldsymbol{\Gamma}}_{II}^{-1} (\boldsymbol{D}_{II}^{C(N_C)})^{-1} \{ [\tilde{\boldsymbol{P}}_I \tilde{\boldsymbol{U}} - \boldsymbol{D}_I^{C(N_C)} \tilde{\boldsymbol{\Gamma}}_I] \boldsymbol{A}_I^{C(N_C)} + (\tilde{\boldsymbol{P}}_I \tilde{\boldsymbol{V}} + \tilde{\boldsymbol{P}}_{II}) [\boldsymbol{A}_{II}^{R(1)}] \}. \tag{20}$$

This equation relates the amplitudes of the waves in the slices at the second junction. Using the results of Eq. (16), we can eliminate the coefficient vectors $\boldsymbol{A}_I^{C(N_C)}$ and $\boldsymbol{A}_{II}^{C(N_C)}$ and find the following four-terminal scattering matrix equation:

$$\begin{bmatrix} [\boldsymbol{A}_I^{R(1)}] \\ [\boldsymbol{A}_{II}^{L(1)}] \end{bmatrix} = \begin{pmatrix} \boldsymbol{\Sigma}_{11}^{4T} & \boldsymbol{\Sigma}_{12}^{4T} \\ \boldsymbol{\Sigma}_{21}^{4T} & \boldsymbol{\Sigma}_{22}^{4T} \end{pmatrix} \begin{bmatrix} [\boldsymbol{A}_I^{L(1)}] \\ [\boldsymbol{A}_{II}^{R(1)}] \end{bmatrix}, \tag{21}$$

with

$$\boldsymbol{\Sigma}_{11}^{4T} = \tilde{\boldsymbol{U}} \{ \boldsymbol{S}_{11}^{3T} + \boldsymbol{S}_{12}^{3T} \tilde{\boldsymbol{X}} [\tilde{\boldsymbol{P}}_I \tilde{\boldsymbol{U}} - \boldsymbol{D}_I^{C(N_C)} \tilde{\boldsymbol{\Gamma}}_I] \boldsymbol{S}_{11}^{3T} \},$$

$$\boldsymbol{\Sigma}_{12}^{4T} = \tilde{\boldsymbol{U}} \boldsymbol{S}_{12}^{3T} \tilde{\boldsymbol{X}} (\tilde{\boldsymbol{P}}_I \tilde{\boldsymbol{V}} + \tilde{\boldsymbol{P}}_{II}) + \tilde{\boldsymbol{V}},$$

$$\boldsymbol{\Sigma}_{21}^{4T} = \boldsymbol{S}_{22}^{3T} \tilde{\boldsymbol{X}} [\tilde{\boldsymbol{P}}_I \tilde{\boldsymbol{U}} - \boldsymbol{D}_I^{C(N_C)} \tilde{\boldsymbol{\Gamma}}_I] \boldsymbol{S}_{11}^{3T} + \boldsymbol{S}_{21}^{3T},$$

$$\boldsymbol{\Sigma}_{22}^{4T} = \boldsymbol{S}_{22}^{3T} \tilde{\boldsymbol{X}} (\tilde{\boldsymbol{P}}_I \tilde{\boldsymbol{V}} + \tilde{\boldsymbol{P}}_{II}), \tag{22}$$

where

$$\tilde{\boldsymbol{U}} = \{ \tilde{\boldsymbol{Q}}_I - \tilde{\boldsymbol{R}}_{II} [\boldsymbol{D}_{II}^{C(N_C)}]^{-1} \tilde{\boldsymbol{P}}_I \}^{-1} \{ \tilde{\boldsymbol{R}}_I - \tilde{\boldsymbol{R}}_{II} [\boldsymbol{D}_{II}^{C(N_C)}]^{-1} \boldsymbol{D}_I^{C(N_C)} \} \tilde{\boldsymbol{\Gamma}}_I,$$

$$\tilde{\boldsymbol{V}} = \{ \tilde{\boldsymbol{Q}}_I - \tilde{\boldsymbol{R}}_{II} [\boldsymbol{D}_{II}^{C(N_C)}]^{-1} \tilde{\boldsymbol{P}}_I \}^{-1} \{ \tilde{\boldsymbol{R}}_{II} [\boldsymbol{D}_{II}^{C(N_C)}]^{-1} \tilde{\boldsymbol{P}}_{II} - \tilde{\boldsymbol{Q}}_{II} \},$$

$$\tilde{\boldsymbol{X}} = \{ \mathbb{1} - \tilde{\boldsymbol{\Gamma}}_{II}^{-1} [\boldsymbol{D}_{II}^{C(N_C)}]^{-1} [\tilde{\boldsymbol{P}}_I \tilde{\boldsymbol{U}} - \boldsymbol{D}_I^{C(N_C)} \tilde{\boldsymbol{\Gamma}}_I] \boldsymbol{S}_{12}^{3T} \}^{-1} \tilde{\boldsymbol{\Gamma}}_{II}^{-1} [\boldsymbol{D}_{II}^{C(N_C)}]^{-1}. \tag{23}$$

Equation (21) relates the amplitudes of the outgoing and decaying waves to the amplitudes of the incoming and exploding waves in the first slices of branches 1–4. This scattering matrix equation can now be iterated by the standard procedure over branches 3 and 4 simultaneously to give the full scattering matrix equation of the four-terminal system,

$$\begin{Bmatrix} [\boldsymbol{A}_I^{R(N)}] \\ [\boldsymbol{A}_{II}^{L(1)}] \end{Bmatrix} = \begin{pmatrix} \boldsymbol{S}_{11}^{4T} & \boldsymbol{S}_{12}^{4T} \\ \boldsymbol{S}_{21}^{4T} & \boldsymbol{S}_{22}^{4T} \end{pmatrix} \begin{Bmatrix} [\boldsymbol{A}_I^{L(1)}] \\ [\boldsymbol{A}_{II}^{R(N)}] \end{Bmatrix}. \tag{24}$$

By setting the first slices in branches 1 and 2, as the two left leads, and the final slices in branches 3 and 4, as the two right leads, this four-terminal scattering matrix equation describes the relations between the amplitudes of the outgoing and incoming waves in the four connecting leads of a four-terminal structure.

D. Transmissions and spin-polarization vectors

Once the scattering matrix $\boldsymbol{S}^{\mathrm{MT}}$ of a multiterminal system has been calculated, the complete scattered wave function of the system is given and, hence, any physical quantity in the system can be calculated. In particular, we are interested in the spin-dependent transport properties, which are characterized by the spin-resolved complex transmission amplitudes from lead λ to λ',

$$t_{\alpha'_{\lambda'}, \alpha_\lambda} = \sqrt{\left| \frac{v_{\alpha'_{\lambda'}}}{v_{\alpha_\lambda}} \right|} (\boldsymbol{S}^{\mathrm{MT}})_{\alpha'_{\lambda'}, \alpha_\lambda}. \tag{25}$$

From these transmission amplitudes, the multiterminal transmission probability $T^{\lambda'\lambda}$ and electron flux polarization vector $\boldsymbol{P}^{\lambda'\lambda}$ can be calculated by a straightforward generalization of the two-terminal results of Ref. 42. For a derivation of the flux polarization vector of a multiterminal hole system, we refer to Sec. IV.

We note that the presented formalism gives an exact solution to the spin-dependent transport of a multiterminal system. For a numerical implementation, the complete expansion basis of infinite dimension in Eq. (2) has to be truncated at a finite value $\mathcal{N}$. Due to the completeness of the basis set, the data converges to the exact limit for large $\mathcal{N}$. In the calculations, we have made $\mathcal{N}$ as large as necessary to obtain a desired numerical accuracy.

III. ELECTRONS

We now apply our derived formalism to study coherent multiterminal electron-spin transport properties in a three- and four-terminal junction (Fig. 1) created by, e.g., lithographic techniques in a two-dimensional electron gas. In the central branch a local Rashba SOI $\alpha(\boldsymbol{r})$ exists. This interaction can be induced by a top gate, creating a local structure-inversion asymmetry of the confinement well. Taking the Cartesian z axis along the heterostructure growth direction, the Hamiltonian, in atomic units, of the system is given by

$$H = \frac{p^2}{2m^*} + V(\boldsymbol{r}) + \frac{1}{2} [\alpha(\boldsymbol{r})(\sigma_x p_y - \sigma_y p_x) + \mathrm{H.c.}], \tag{26}$$

with velocity operator $v_x = p_x/m^* - \alpha(\boldsymbol{r})\sigma_y$. Branches 1, 2, and C for the three-terminal structure, as well as branches 1 to 4 for the four-terminal structure, are connected to perfect leads of transverse width w with vanishing spin-orbit interaction.

In Fig. 2, we show the calculated flux polarization vector of a cross section in leads 1 and 2 of the three-terminal structure shown in the left part of Fig. 1, resulting from an unpolarized injection of carriers in the central branch. Due to the vanishing SOI in the leads the polarization is independent of the longitudinal position in the leads. Here the junction connecting leads 1 and 2 with the central lead is taken to be $5w$ long. In the junction the local Rashba SOI is taken to be constant and of strength $\alpha = 0.2\pi^2/wm^*$. Similar to the spin

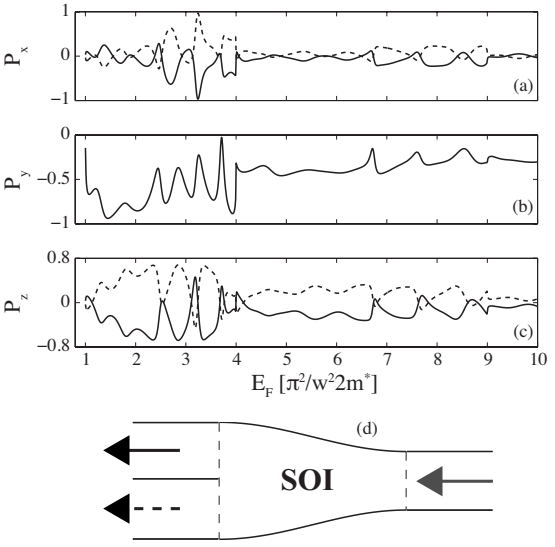

FIG. 2. (a)–(c) Electron flux polarization components in leads 1 (solid line) and 2 (dashed line) of the three-terminal structure due to an unpolarized injection in the central branch as a function of the Fermi energy of the carriers. The x and z components show an antisymmetry between the two outgoing leads, whereas the y components are identical in the two leads. (d) Schematic indicating the incoming and outgoing fluxes and area of nonzero SOI.

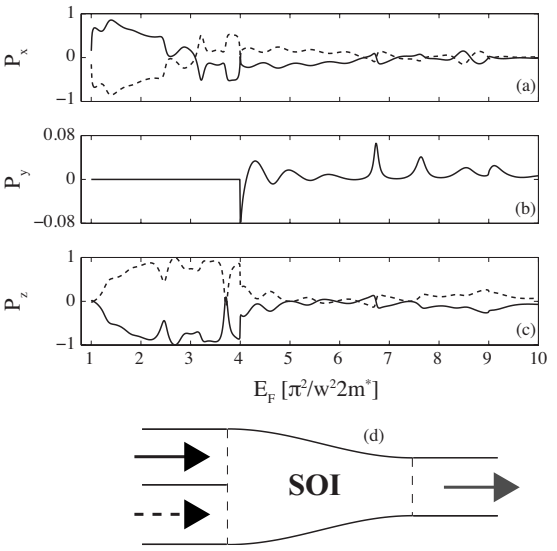

FIG. 3. (a)–(c) Electron flux polarization components in the central lead due to an unpolarized injection in branches 1 (solid line) and 2 (dashed line) as a function of the Fermi energy of the carriers. The x and z components show an antisymmetry between injections in the two leads, whereas the y components resulting from the injections in the two leads are identical. It is also seen that y components are zero when only one doubly-degenerate channel is available in the central lead. (d) Schematic indicating the incoming and outgoing fluxes and area of nonzero SOI.

accumulation along the transverse edges of a waveguide akin to the spin Hall effect,[43,44] we observe that the x and z components, respectively, [Figs. 2(a) and 2(c)] are nonzero and antisymmetric in the two outgoing leads. This contrasts the two-terminal transport where, due to the reflection symmetry, the x and z components vanish identically.[42] However, considering the polarization in branches 1 and 2 combined, the antisymmetry implies the two-terminal result of the vanishing spin-polarization components along the x and z directions. The y components, on the other hand, are identical in the two leads and are therefore nonzero, even when considering the combined polarization of both branches. This is consistent with the symmetric spin accumulations along the edges of a waveguide projected in the transverse direction found in Ref. 43. We note that all polarization components are nonzero in the single spin-degenerate channel regime as opposed to the two-terminal results[42,45,46] since the coherent superposition of the outgoing state in the two branches supply two spin-degenerate channels.

We now turn to the study of transport in the opposite direction, i.e., injections in branches 1 and 2. Figure 3 shows the spin-polarization components of the outgoing flux in the central branch for an unpolarized injection in branch 1 (solid line) and for an unpolarized injection in branch 2 (dashed line). It is seen that the x component of the polarization in the central branch [Fig. 3(a)] resulting from an unpolarized injection in branch 1 is antisymmetric to the polarization, resulting from an injection of unpolarized carriers in branch 2. For a simultaneous injection of unpolarized carriers in branches 1 and 2, the resulting polarization vanishes. This is also true for the z component of the polarization shown in Fig. 3(c). The induced y component of the polarization in Fig. 3(b) is identical for injection in branches 1 and 2. This therefore naturally gives a finite transverse polarization component from a simultaneous injection in branches 1 and 2. However, here the y components are only nonzero, when the central lead supports more than one spin-degenerate channel. We see that Figs. 2 and 3 imply a spin-polarization rectification in the y component between unpolarized injections in the central branch and in branches 1 and 2, similar to what was found in a two-terminal horn structure.[47]

An interesting observation from the results of Figs. 2 and 3 is that by measuring transport between, e.g., branches 1 and C, the presence of a third lead allows a finite polarization to be achieved in the single spin-degenerate channel regime of the outgoing lead. This is in strong contrast to a two-terminal system where the time-reversal symmetry constrains the polarization components to vanish for single-channel transport.[42,45,46]

Let us analytically prove the results observed in the numerical calculations. Assuming the eigenmodes in the leads to be normalized by their velocities and applying the Einstein summation convention, we can write the scattering matrix for the considered three-terminal system as

$$\begin{pmatrix} a^{1,II}_{n_1\sigma_1} \\ a^{2,II}_{n_2\sigma_2} \\ a^{C,I}_{n_C\sigma_C} \end{pmatrix} = \begin{pmatrix} t^{1C}_{n_1\sigma_1,n'_C\sigma'_C} & r^{1}_{n_1\sigma_1,n'_1\sigma'_1} & t^{12}_{n_1\sigma_1,n'_2\sigma'_2} \\ t^{2C}_{n_2\sigma_2,n'_C\sigma'_C} & t^{21}_{n_2\sigma_2,n'_1\sigma'_1} & r^{2}_{n_2\sigma_2,n'_2\sigma'_2} \\ r^{C}_{n_C\sigma_C,n'_C\sigma'_C} & t^{C1}_{n_C\sigma_C,n'_1\sigma'_1} & t^{C2}_{n_C\sigma_C,n'_2\sigma'_2} \end{pmatrix} \begin{pmatrix} a^{C,II}_{n'_C\sigma'_C} \\ a^{1,I}_{n'_1\sigma'_1} \\ a^{2,I}_{n'_2\sigma'_2} \end{pmatrix}. \tag{27}$$

The Hamiltonian is symmetric under the operation $\sigma_y R_y$ with R_y being the reflection operator in the transverse direction.

This operation maps the eigenmodes of leads 1 and 2 onto each other, such that

$$\sigma_y R_y : \phi_{n_1\sigma_1}(y)^{1,I\{II\}} \rightarrow i\bar{\sigma}_1(-1)^{n_1}\phi_{n_1\bar{\sigma}_1}(-y)^{2,I\{II\}}$$

and conversely

$$\sigma_y R_y : \phi_{n_2\sigma_2}(y)^{2,I\{II\}} \rightarrow i\bar{\sigma}_2(-1)^{n_2}\phi_{n_2\bar{\sigma}_2}(-y)^{1,I\{II\}},$$

whereas the eigenmodes of the central lead naturally maps onto themselves

$$\sigma_y R_y : \phi_{n_C\sigma_C}(y)^{C,I\{II\}} \rightarrow i\bar{\sigma}_C(-1)^{n_C}\phi_{n_C\bar{\sigma}_C}(-y)^{C,I\{II\}}.$$

By considering these transformations,[42] we find that the scattering matrix must satisfy

$$\begin{bmatrix} i\bar{\sigma}_1(-1)^{n_1}a^{2,II}_{n_1\bar{\sigma}_1} \\ i\bar{\sigma}_2(-1)^{n_2}a^{1,II}_{n_2\bar{\sigma}_2} \\ i\bar{\sigma}_C(-1)^{n_C}a^{C,I}_{n_C\bar{\sigma}_C} \end{bmatrix} = \begin{pmatrix} t^{1C}_{n_1\sigma_1,n'_C\sigma'_C} & r^{1}_{n_1\sigma_1,n'_1\sigma'_1} & t^{12}_{n_1\sigma_1,n'_2\sigma'_2} \\ t^{2C}_{n_2\sigma_2,n'_C\sigma'_C} & t^{21}_{n_2\sigma_2,n'_1\sigma'_1} & r^{2}_{n_2\sigma_2,n'_2\sigma'_2} \\ r^{C}_{n_C\sigma_C,n'_C\sigma'_C} & t^{C1}_{n_C\sigma_C,n'_1\sigma'_1} & t^{C2}_{n_C\sigma_C,n'_2\sigma'_2} \end{pmatrix} \times \begin{bmatrix} i\bar{\sigma}_C(-1)^{n_C}a^{C,II}_{n'_C\bar{\sigma}'_C} \\ i\bar{\sigma}'_1(-1)^{n'_1}a^{2,I}_{n'_1\bar{\sigma}'_1} \\ i\bar{\sigma}'_2(-1)^{n'_2}a^{1,I}_{n'_2\bar{\sigma}'_2} \end{bmatrix}. \quad (28)$$

Comparing Eq. (27) with Eq. (28), we find that the transmission amplitudes satisfy

$$t^{1C}_{n_1\sigma_1,n_C\sigma_C} = (-1)^{n_1+n_C}\sigma_1\sigma_C t^{2C}_{n_1\bar{\sigma}_1,n_C\bar{\sigma}_C},$$

$$t^{C2}_{n_C\sigma_C,n_2\sigma_2} = (-1)^{n_2+n_C}\sigma_2\sigma_C t^{C1}_{n_C\bar{\sigma}_C,n_2\bar{\sigma}_2}. \quad (29)$$

For the injection in the central branch this implies the constraints on the spin-resolved conductance and flux polarization,

$$G^{1C}_{\sigma'\sigma} = G^{2C}_{\bar{\sigma}'\bar{\sigma}},$$

$$P^{1C}_{x,z} = -P^{2C}_{x,z},$$

$$P^{1C}_{y} = P^{2C}_{y}. \quad (30)$$

This shows that the antisymmetric polarizations along the x and z directions and the equality of the y components induced in branches 1 and 2 in Fig. 2 are rigorous results of the symmetry constraints of the system. Here, the nonvanishing x and z components, which are not found in a transversely symmetric two-terminal system, arise due to the effective symmetry breaking by the projection onto branch 1 or 2. Furthermore, since a measurement of the flux polarization in one of the outgoing branches immediately gives the polarization in the other outgoing branch, the spin flux in the two branches are entangled by symmetry. From Eq. (29), we can also deduce the constraints on the spin-resolved conductances and flux polarizations for the transport from branches 1 and 2 into the central branch,

$$G^{C1}_{\sigma'\sigma} = G^{C2}_{\bar{\sigma}'\bar{\sigma}},$$

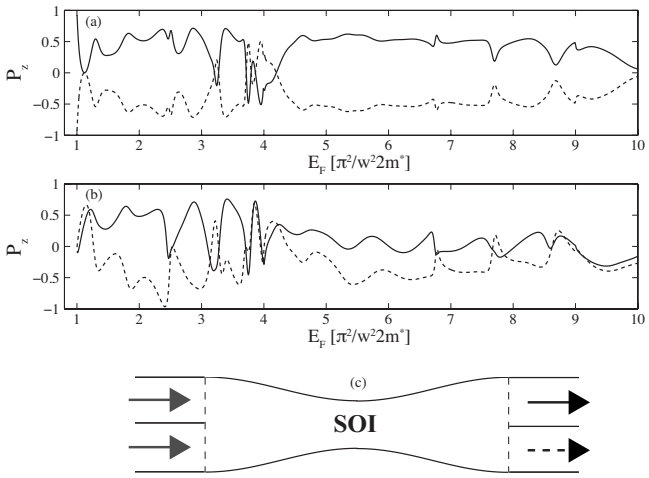

FIG. 4. (a) and (b) Electron flux polarization components in a four-terminal junction as a function of Fermi energy for spin-polarized injection. (a) Polarization in lead 3 (solid line) and lead 4 (dashed line) for simultaneous injection of spin-up polarized electrons in branch 1 and spin-down polarized carriers in branch 2. (b) Same as (a) except for spin-up polarized injected carriers in both branches 1 and 2. The four-terminal structure is able to partition a fully spin-polarized flux into two largely oppositely-polarized fluxes. (c) Schematic figure indicating the incoming and outgoing fluxes and area of nonzero SOI.

$$P^{C1}_{x,z} = -P^{C2}_{x,z},$$

$$P^{C1}_{y} = P^{C2}_{y}. \quad (31)$$

These constraints confirm the symmetries of the polarization shown in Fig. 3.

Consider now a four-terminal structure created by connecting two three-terminal structures back-to-back indicated in Fig. 1. It is straightforward to generalize the above symmetry consideration to the four-terminal structure giving the constraints

$$t^{31}_{n_3\sigma_3,n_1\sigma_1} = (-1)^{n_1+n_3}\sigma_1\sigma_3 t^{42}_{n_3\bar{\sigma}_3,n_1\bar{\sigma}_1},$$

$$t^{41}_{n_4\sigma_4,n_1\sigma_1} = (-1)^{n_1+n_4}\sigma_1\sigma_4 t^{32}_{n_4\bar{\sigma}_4,n_1\bar{\sigma}_1}. \quad (32)$$

For the injection of unpolarized carriers in both branches 1 and 2, these constraints imply antisymmetric x and z polarization components and identical y components in the outgoing branches 3 and 4.

As seen in Fig. 4(a), this is also true if branches 1 and 2 are injected with carriers of opposite polarization, e.g, spin up in branch 1 and spin down in branch 2. This follows since the $\sigma_y R_y$ symmetry operation maps a spin-up mode in lead 1 onto a spin-down mode in lead 2, and similarly for leads 3 and 4 (see the symmetry discussion of the three-terminal system). However, this symmetry is broken by injecting the two branches with carriers of the same polarization, e.g., spin up in both branches 1 and 2. This is seen in Fig. 4(b) as an asymmetric polarization in the outgoing branches 3 and 4. Here, although the outgoing polarizations are not constrained by symmetry to be opposite, we see that the four-terminal

structure can create two largely oppositely-polarized fluxes from a completely spin-polarized flux, e.g., a spin-up polarized flux in leads 3 and a spin-down polarized flux in branch 4 from the injection of spin-up polarized carriers in branches 1 and 2.

IV. HOLES

We now turn our attention to the much less studied field of hole transport in nanostructures. To this end we will consider a three-terminal structure (Fig. 1), with the same dimensions as considered for the electron transport in Sec. III, in a two-dimensional GaAs hole gas, grown along the crystallographic [001] direction. We again take the Cartesian z axis to be parallel with the growth direction. The 4×4 Luttinger Hamiltonian[48] in atomic units, describing the heavy- and light-hole semiconductor valence bands then reads

$$H=\frac{\tilde{\gamma}_1}{2}\Pi^2-\gamma_2(J_x^2\Pi_x^2+J_y^2\Pi_y^2+J_z^2p_z^2)-\frac{\gamma_3}{2}(\{J_x,J_y\}\{\Pi_x,\Pi_y\}+\{J_x,J_z\}\{\Pi_x,\Pi_z\}+\{J_z,J_y\}\{\Pi_z,\Pi_y\})+2\kappa\mu_B\boldsymbol{B}\cdot\boldsymbol{J}+V(\boldsymbol{r}), \tag{33}$$

where γ_i and κ are bulk band parameters,[49] $\tilde{\gamma}_1=\gamma_1+5\gamma_2/2$ and J_i are the 4×4 angular-momentum matrices,[50] and the kinetic momentum $\Pi_i=p_i+A_i$. The grown heterostructure quantum well is assumed to be of square geometry with width $a_z=0.05w$, where w is the smallest transverse confinement width in the structure (i.e., the leads connecting the branches). The Hamiltonian is projected onto the lowest state in the growth direction with $\langle p_z^2\rangle=\pi^2/a_z^2$ and $\langle p_z\rangle=0$.

We will consider two magnetic-field orientations: in the out-of-plane z direction and in the in-plane transverse y direction. The field strength is taken to be $B=10^{-3}\langle p_z^2\rangle$. For the out-of-plane direction, we choose the vector potential $\boldsymbol{A}=-yB_z\hat{x}$. For the in-plane field direction, the ratio of the magnetic length to the confinement length is $\sqrt{l_B^2/a_z^2}=\sqrt{\langle p_z^2\rangle/\pi^2B}=\sqrt{10^3/\pi^2}$. The vector potential contribution is, in this case, negligible and we therefore take $\boldsymbol{A}=\boldsymbol{0}$ for the in-plane field direction.

The system is again divided into slices and the eigensolution in each slice is assumed on the form of Eq. (1) with a four-component spinor basis. To find the scattering wave function at a given Fermi energy, we map the Schrödinger equation to an eigenequation in the wave numbers as

$$\begin{pmatrix}\boldsymbol{0} & \boldsymbol{R}^{-1}\\ \boldsymbol{S} & \boldsymbol{T}\end{pmatrix}\begin{pmatrix}\boldsymbol{d}\\ \boldsymbol{f}\end{pmatrix}=k_\alpha\begin{pmatrix}\boldsymbol{d}\\ \boldsymbol{f}\end{pmatrix}, \tag{34}$$

with

$$(\boldsymbol{d})_{n\sigma,\alpha}=d_{n\sigma,\alpha},\quad \boldsymbol{f}=k_\alpha\boldsymbol{R}\boldsymbol{d},$$

$$\boldsymbol{R}=\left(\frac{\gamma_1}{2}\mathbb{1}-\gamma_2J_x^2\right)\otimes\mathbb{1},$$

$$\boldsymbol{S}=\mathbb{1}\otimes\left(E_F\mathbb{1}-\frac{\gamma_1}{2}[p_y^2+A_x^2+\langle p_z^2\rangle\mathbb{1}]\right)+\gamma_2(J_y^2\otimes p_y^2+J_x^2\otimes A_x^2+\langle p_z^2\rangle J_z^2\otimes\mathbb{1}),$$

$$+\gamma_3\{J_x,J_y\}\otimes A_xp_y-2\kappa\mu_B\boldsymbol{B}\cdot\boldsymbol{J}\otimes\mathbb{1},$$

$$\boldsymbol{T}=\left[\gamma_3\{J_x,J_y\}\otimes p_y-\left(\frac{\tilde{\gamma}_1}{2}\mathbb{1}-\gamma_2J_x^2\right)\otimes2A_x\right]\boldsymbol{R}^{-1}. \tag{35}$$

We note that p_y, p_y^2, A_x, A_x^2, and A_xp_y here are matrix representations of the operators in the chosen spatial basis. The states are separated into two sets, I and II, as $I=\{\alpha|\Im(k_\alpha)=0\wedge v_\alpha>0\vee\Im(k_\alpha)>0\}$ and $II=\{\alpha|\Im(k_\alpha)=0\wedge v_\alpha<0\vee\Im(k_\alpha)<0\}$. Using the velocity operator derived directly from the Hamiltonian,

$$v_x=i[H,x]=(\tilde{\gamma}_1\mathbb{1}-2\gamma_2J_x^2\otimes\mathbb{1})p_x-\gamma_3\{J_x,J_y\}\otimes p_y+\left(\frac{\tilde{\gamma}_1}{2}\mathbb{1}-\gamma_2J_x^2\right)\otimes2A_x, \tag{36}$$

we can calculate the expectation value of v_x for the eigenstate corresponding to the wave number k_α as

$$v_\alpha=\langle v_x(k_\alpha)\rangle=\sum_{\sigma'm,\sigma n}(d_{\sigma'm,\alpha})^*\langle\chi_{\sigma'm}|(\tilde{\gamma}_1\mathbb{1}-2\gamma_2J_x^2\otimes\mathbb{1})k_\alpha-\gamma_3\{J_x,J_y\}\otimes p_y+\left(\frac{\tilde{\gamma}_1}{2}\mathbb{1}-\gamma_2J_x^2\right)\otimes2A_x|\chi_{\sigma n}\rangle d_{\sigma n,\alpha}=\boldsymbol{d}_\alpha^\dagger\boldsymbol{v}(k_\alpha)\boldsymbol{d}_\alpha, \tag{37}$$

where $\boldsymbol{v}(k_\alpha)$ is the matrix representation of the velocity operator, in the chosen representation, used to construct the $\boldsymbol{Q}$ matrices in the scattering matrix formalism.

In our calculations we will not make any simplifying assumptions on the leads but rather calculate the true eigenstates from the Luttinger Hamiltonian [Eq. (33)]. Corrections found in the Kane Hamiltonian[49] are straightforward to implement by adding the necessary terms in Eq. (35) and the velocity operator of Eq. (36).

We now move on to derive the polarization vector for the hole system. The density matrix for an injected state in branch C normalized to unit velocity can be written as

$$\boldsymbol{\rho}_\alpha^C=\sum_{\sigma n,\sigma'm}\frac{d_{\sigma n,\alpha}^Cd_{\sigma'm,\alpha}^{C*}}{v_\alpha}|\sigma n\rangle\langle\sigma'm|. \tag{38}$$

Each mode is injected incoherently, and the angular-momentum expectation value is given by

$$\langle\boldsymbol{J}\rangle_C=\frac{\sum_\alpha\mathrm{Tr}(\boldsymbol{J}\boldsymbol{\rho}_\alpha^C)}{\sum_\alpha1/v_\alpha}=\frac{\sum_{\alpha,\sigma\sigma'n}d_{\sigma n,\alpha}^Cd_{\sigma'n,\alpha}^{C*}\langle\sigma'|\boldsymbol{J}|\sigma\rangle/v_\alpha}{\sum_\alpha1/v_\alpha}, \tag{39}$$

with the sum over α taken over the propagating modes, i.e., with $\Im(k_\alpha)=0$. The density matrix for the outgoing state in the lead connecting branch $\lambda=1$ or 2 is given by

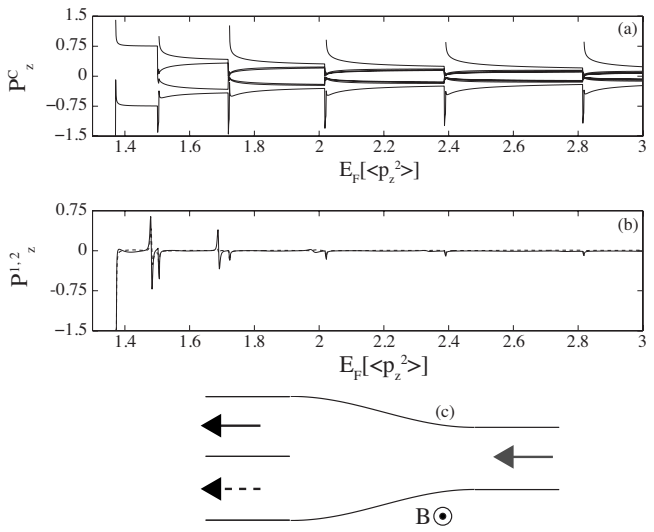

FIG. 5. Hole polarization as a function of the Fermi energy at $B_z=10^{-3}\langle p_z^2\rangle$ of (a) injected states in the central branch, and (b) outgoing states in leads 1 (solid line) and 2 (dashed line). (c) Schematic figure indicating the incoming and outgoing fluxes and direction of the magnetic field.

$$\boldsymbol{\rho}^{\lambda} = \frac{1}{T^{\lambda C}} \sum_{\beta,\alpha\sigma n,\alpha'\sigma' m} \frac{\sqrt{v_\alpha v_{\alpha'}}}{|v_\beta|} (S^{3T})_{\alpha,\beta} (S^{3T})^*_{\alpha',\beta} \times e^{i(k_\alpha - k_{\alpha'})x} d^{\lambda}_{\sigma n,\alpha} d^{\lambda *}_{\sigma' m,\alpha'} |\sigma n\rangle\langle \sigma' m|, \tag{40}$$

where $T^{\lambda C}$ is the transmission probability from lead C to λ. From this, the angular-momentum expectation value can be calculated as

$$\langle \boldsymbol{J}\rangle_{\lambda} = \frac{1}{T^{\lambda C}} \sum_{\beta,\alpha\sigma n,\alpha'\sigma'} \frac{\sqrt{v_\alpha v_{\alpha'}}}{|v_\beta|} (S^{3T})_{\alpha,\beta} (S^{3T})^*_{\alpha',\beta} \times e^{i(k_\alpha - k_{\alpha'})x} d^{\lambda}_{\sigma n,\alpha} d^{\lambda *}_{\sigma' n,\alpha'} \langle \sigma'|\boldsymbol{J}|\sigma\rangle. \tag{41}$$

In Fig. 5(a), we show the polarization of the injected states in the central branch for a weak magnetic field applied in the out-of-plane z direction, $B_z=10^{-3}\langle p_z^2\rangle$ (Ref. 51). A pure heavy-hole (light-hole) state has $P_z=\pm 3/2(\pm 1/2)$. Deviation from these values therefore indicates a state with mixed heavy-light-hole character. For the first Zeeman-split subband, the injected mode shows $P_z=-3/2$, being a pure heavy-hole state polarized along the magnetic-field direction. This is consistent with the results for two-dimensional hole gases at small wave numbers,[49] relevant here due to the lead width to heterostructure-well width ratio $w/a_z=20$. In the single-channel energy regime, the complete flux is naturally carried by this single mode. As the second channel of the Zeeman-split pair open for transport, the injected flux is distributed—unequally—on both channels, and the angular-momentum contribution carried by each individual channel is reduced. The polarization vector amplitude of each channel is therefore reduced and saturates at $P_z\approx\pm 0.75$ for Fermi energies well above the subband edge. As the Fermi energy $E_F\to\infty$, each channel carries an infinitesimal angular momentum, implying a vanishing amplitude of each channel

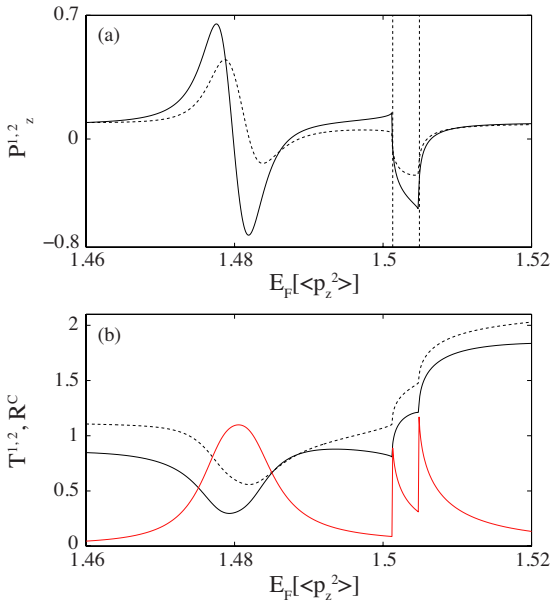

FIG. 6. (Color online) (a) First peak structures of Fig. 5 in finer scale with vertical dashed lines indicating the third and fourth subband edges. (b) Transmission probability from the central branch to branches 1 (black thick solid line) and 2 (black thick dashed line) and reflection into the central branch (thin red line). Antisymmetric peak dip in polarization corresponding to the transmission dip close to the subband edge indicating the angular-momentum dependent Fano scattering in the three-terminal junction.

polarization vector (see $E_F=3\langle p_z^2\rangle$ in Fig. 5). We see that, except at the onset of conducting channels where the small Zeeman-energy split is most pronounced, the polarization of the modes is opposite to each other. Since for multimode transport all available channels are injected incoherently, the polarization of the injected state is the vector addition of the individual mode contributions. The complete injected state is therefore unpolarized at $B\to 0$.

The polarizations of the outgoing states in branches 1 and 2 are shown in Fig. 5(b) (Ref. 51). When only one split channel is open, the available state is pure and the angular-momentum expectation value of the outgoing state reduces to

$$\langle \boldsymbol{J}\rangle^{\lambda}_{\text{single channel}} = \sum_{n\sigma\sigma'} d^{\lambda}_{n\sigma,1} d^{\lambda *}_{n\sigma',1} \langle \sigma'|\boldsymbol{J}|\sigma\rangle, \tag{42}$$

which is just the expectation value of the lowest state in the lead, independent of the transmission properties, and hence the nature of scattering in the junction. The outgoing state is therefore a pure heavy-hole state, similar to the injected state. This is true as long as only the first channel is open. As the second channel opens, the outgoing polarization sharply drops close to zero, and remains so until the third and fourth channel open up. At this subband edge and at each consecutive subband edge, an asymmetric peak-dip structure followed by a dip is found in the polarization. Figure 6(a) reveals that the peak-dip structure appears below the subband edge and the following dip lies between the Zeeman-split subband edges. Looking at the transmission probability in

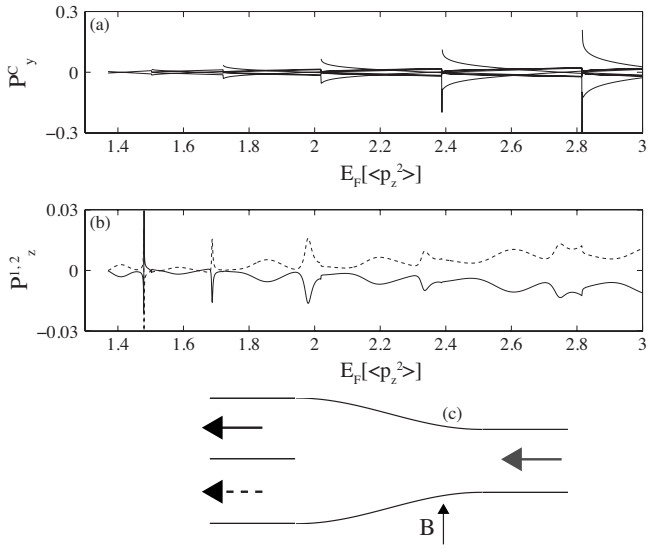

FIG. 7. Hole polarization as a function of the Fermi energy at $B_y=10^{-3}\langle p_z^2\rangle$ of (a) injected states in the central branch and (b) outgoing states in leads 1 (solid line) and 2 (dashed line). Outgoing states oppositely polarized by symmetry. (c) Schematic figure indicating the incoming and outgoing fluxes and direction of the magnetic field.

Fig. 6(b), we see that the peak dip in the polarization is accompanied by a dip in the transmission probability. This suggest that this feature is related to an angular-momentum Fano resonance due to interaction with localized states in the three-terminal junction.[38,52]

For a weak magnetic field applied in the transverse y direction, $B_y=10^{-3}\langle p_z^2\rangle$, the injected states show weak polarization along the transverse field [see Fig. 7(a)]. However, the outgoing state [Fig. 7(b)] is largely polarized in the out-of-plane z direction[53] with an antisymmetry between branches 1 and 2. This symmetry contrasts a magnetic field applied in the out-of-plane direction (Figs. 5 and 6), where the outgoing polarization did not carry any symmetry. A symmetry between branches 1 and 2 implies conservation of an operator U, containing the transverse reflection. From $\{J_x,J_y\}=\sqrt{3}\sigma_y\otimes\mathbb{1}$, we then know that in order for U to commute with the Luttinger Hamiltonian, it needs to be on the form $U=(\sigma_x\otimes\boldsymbol{m})R_y$ or $U=(\sigma_z\otimes\boldsymbol{m})R_y$, with $\boldsymbol{m}$ being some 2×2 matrix. From $J_x^2=(\sqrt{3}/2)\sigma_x\otimes\mathbb{1}-(1/2)\sigma_z\otimes\sigma_z+(5/4)$, we see that the only possibilities are $U=(\sigma_x\otimes\sigma_x)R_y$ or $U=(\sigma_x\otimes\sigma_y)R_y$ (Ref. 54). We have thus found all the possible symmetries of the Luttinger Hamiltonian at $B=0$, containing a transverse reflection. With a magnetic field in the x or y direction, the possible symmetry operators are reduced to $U=(\sigma_x\otimes\sigma_x)R_y$ or $U=(\sigma_x\otimes\sigma_y)R_y$, respectively. For a magnetic field in the z direction, due to the fact that $J_z=\sigma_z\otimes\mathbb{1}+(1/2)\mathbb{1}\otimes\sigma_z$, there is no operator containing reflection symmetry, which commutes with the Hamiltonian implying the observed absence of symmetry in Figs. 5 and 6.

V. CONCLUSION

The presented spin-dependent multichannel multiterminal scattering matrix method provides an exact solution to the spin-dependent quantum transport problem. It has been derived in such a way as to provide an efficient and stable numerical implementation. The method can, e.g., be applied to study coherent spin currents and polarization, spin-dependent noise and entanglement, spin accumulations, phase properties, etc., in multiterminal structures. By applying this method, it showed how the coherent nature of the scattered carriers and the existence of multiple terminals, affect the polarization properties in comparison with the previously derived two-terminal results. We furthermore showed a polarization-rectification effect for electrons in a three-terminal structure with a local Rashba spin-orbit interaction. A fully spin-polarized flux can be partitioned into a spin-up and a spin-down polarized flux, utilizing a four-terminal junction with SOI.

For holes the polarization of the outgoing state is uniquely determined by the lead states, whenever the outgoing lead only supports a single channel. In a three-terminal structure, the outgoing states are largely unpolarized away from the lead subband edges. Close to the onset of the third and fourth channel, as well as the consecutive channels, the polarization shows peak-dip structures, akin to the angular-momentum Fano resonances in the three-terminal junction.

The considered multiterminal transport properties are expected to be observable in low-temperature measurements in nanoscale structures. These can be realized in, e.g., heterostructure quantum wells by standard lithographic techniques. Assuming the structures to be attached to the leads of width $w=400$ nm, the considered Rashba SOI strength $\alpha\approx10^{-11}$ eVm for an InGaAs host material, which has been demonstrated in gated heterostructures.[55] For the hole systems we have assumed a GaAs host material. With the same lead width as for the electron-transport case and a heterostructure-well width $a_z=20$ nm, the considered magnetic-field strength was $B\approx33$ mT.

ACKNOWLEDGMENTS

This work was supported by the Swedish Research Council (VR) and by the Swedish Foundation for Strategic Research (SSF) through the Nanometer Structure Consortium at Lund University. P.B. is grateful for the hospitality and funding from the Institute of Fundamental Sciences and the MacDiarmid Institute for Advanced Materials and Nanotechnology, Massey University in New Zealand, where part of this work was conducted.

*Patrik.Brusheim@ftf.lth.se
†Hongqi.Xu@ftf.lth.se

[1] M. Büttiker, Phys. Rev. Lett. **57**, 1761 (1986); IBM J. Res. Dev. **32**, 317 (1988).
[2] D. G. Ravenhall, H. W. Wyld, and R. L. Schult, Phys. Rev. Lett. **62**, 1780 (1989).
[3] H. U. Baranger and A. D. Stone, Phys. Rev. Lett. **63**, 414 (1989).
[4] R. L. Schult, H. W. Wyld, and D. G. Ravenhall, Phys. Rev. B **41**, 12760 (1990).
[5] J. B. Xia, Phys. Rev. B **45**, 3593 (1992).
[6] J. Wang, Y. J. Wang, and H. Guo, Phys. Rev. B **46**, 2420 (1992).
[7] O. Vanbésien and D. Lippens, Appl. Phys. Lett. **65**, 2439 (1994).
[8] M. Shin, S. Lee, K. W. Park, and E.-H. Lee, Phys. Rev. B **50**, 11192 (1994).
[9] T. Itoh, Phys. Rev. B **52**, 1508 (1995).
[10] Y. M. Blanter and M. Büttiker, Phys. Rev. B **56**, 2127 (1997).
[11] H. K. Zhao, Phys. Lett. A **226**, 105 (1997).
[12] W. Sheng, J. Phys.: Condens. Matter **9**, 8369 (1997).
[13] W. D. Sheng and H. Q. Xu, J. Appl. Phys. **84**, 2146 (1998).
[14] H. Q. Xu, Appl. Phys. Lett. **78**, 2064 (2001); **80**, 853 (2002).
[15] A. N. Andriotis, M. Menon, D. Srivastava, and L. Chernozatonskii, Phys. Rev. Lett. **87**, 066802 (2001).
[16] H. Q. Xu, Phys. Rev. B **66**, 165305 (2002).
[17] D. Csontos and H. Q. Xu, J. Phys.: Condens. Matter **14**, 12513 (2002); D. Csontos and H. Q. Xu, Phys. Rev. B **67**, 235322 (2003).
[18] D. Mamaluy, M. Sabathil, and P. Vogl, J. Appl. Phys. **93**, 4628 (2003).
[19] A. N. Jordan and M. Büttiker, Phys. Rev. B **77**, 075334 (2008).
[20] K. L. Shepard, M. L. Roukes, and B. P. van der Gaag, Phys. Rev. B **46**, 9648 (1992).
[21] R. de Picciotto, H. L. Stormer, L. N. Pfeiffer, K. W. Baldwin, and K. W. West, Nature (London) **411**, 51 (2001).
[22] I. Shorubalko, H. Q. Xu, I. Maximov, P. Omling, L. Samuelson, and W. Seifert, Appl. Phys. Lett. **79**, 1384 (2001).
[23] L. Worschech, H. Q. Xu, A. Forchel, and L. Samuelson, Appl. Phys. Lett. **79**, 3287 (2001).
[24] R. Leturcq, D. Graf, T. Ihn, K. Ensslin, D. D. Driscoll, and A. C. Gossard, Europhys. Lett. **67**, 439 (2004).
[25] D. Wallin and H. Q. Xu, Appl. Phys. Lett. **86**, 253510 (2005).
[26] P. R. Bandaru, C. Daraio, S. Jin, and A. M. Rao, Nat. Mater. **4**, 663 (2005).
[27] J. Sun, D. Wallin, P. Brusheim, I. Maximov, Z. G. Wang, and H. Q. Xu, Nanotechnology **18**, 195205 (2007).
[28] T. P. Pareek, Phys. Rev. Lett. **92**, 076601 (2004).
[29] A. A. Kiselev and K. W. Kim, J. Appl. Phys. **94**, 4001 (2003).
[30] H.-F. Lü and Y. Guo, Appl. Phys. Lett. **91**, 092128 (2007).
[31] S. Bellucci and P. Onorato, Phys. Rev. B **77**, 075303 (2008).
[32] J. C. Egues, G. Burkard, and D. Loss, Phys. Rev. Lett. **89**, 176401 (2002).
[33] B. K. Nikolić, S. Souma, L. P. Zârbo, and J. Sinova, Phys. Rev. Lett. **95**, 046601 (2005); B. K. Nikolić, L. P. Zârbo, and S. Souma, Phys. Rev. B **72**, 075361 (2005).
[34] C. P. Moca and D. C. Marinescu, Phys. Rev. B **72**, 165335 (2005).
[35] M. W. Wu and J. Zhou, Phys. Rev. B **72**, 115333 (2005).
[36] M. G. Pala, M. Governale, U. Zülicke, and G. Iannaccone, Phys. Rev. B **71**, 115306 (2005).
[37] P. Brusheim and H. Q. Xu, Phys. Rev. B **73**, 045313 (2006).
[38] L. Zhang, P. Brusheim, and H. Q. Xu, Phys. Rev. B **72**, 045347 (2005).
[39] H. Q. Xu, Phys. Rev. B **50**, 8469 (1994); **52**, 5803 (1995).
[40] L. Zhang, F. Zhai, and H. Q. Xu, Phys. Rev. B **74**, 195332 (2006); **75**, 199902(E) (2007).
[41] To avoid numerical instabilities the derivation should only contain uninverted phase factors of group I, i.e. Γ_{I}, and inverted phase factors of group II, i.e. $\Gamma_{\mathrm{II}}^{-1}$, as well as avoid direct inversion of the matrices **P** and **R** containing the, possibly, badly scaled overlap matrices **F**.
[42] F. Zhai and H. Q. Xu, Phys. Rev. Lett. **94**, 246601 (2005).
[43] P. Brusheim and H. Q. Xu, Phys. Rev. B **74**, 205307 (2006).
[44] P. Brusheim and H. Q. Xu, Phys. Rev. B **75**, 195333 (2007).
[45] E. N. Bulgakov and A. F. Sadreev, Phys. Rev. B **66**, 075331 (2002).
[46] A. A. Kiselev and K. W. Kim, Phys. Rev. B **71**, 153315 (2005).
[47] F. Zhai, K. Chang, and H. Q. Xu, Appl. Phys. Lett. **92**, 102111 (2008).
[48] J. M. Luttinger, Phys. Rev. **102**, 1030 (1956).
[49] R. Winkler, *Spin-Orbit Coupling Effects in Two-Dimensional Electron and Hole Systems* (Springer-Verlag, Berlin, 2003).
[50] S. Murakami, N. Nagaosa, and S.-C. Zhang, Phys. Rev. B **69**, 235206 (2004).
[51] The x and y components are zero.
[52] A. A. Kiselev and K. W. Kim, Appl. Phys. Lett. **78**, 775 (2001).
[53] The polarizations in the x and z directions are $\sim 10^{-3}$ and are not shown here.
[54] P. Brusheim and H. Q. Xu, Phys. Rev. B **74**, 233306 (2006).
[55] J. Nitta, T. Akazaki, H. Takayanagi, and T. Enoki, Phys. Rev. Lett. **78**, 1335 (1997).